Analysis and Design of Microwave Balanced Mixers

BERND SCHÜPPERT

Abstract — **Based on the theory given in [1], planar balanced mixers are analyzed for fundamental and harmonic mixing, mixing product recovery, and the effect of circuit and diode parameters on the conversion loss. The successful incorporation of the proposed method in a CAD procedure is demonstrated through the development of a multioctave balanced mixer with $L = 6$ dB ± 1 dB from 1.5 to 12.75 GHz.**

I. Introduction

IN THE FIELD OF mixer research, there are only a few publications which deal with theoretical *and* experimental results [2]–[5]. This paper is intended to give a comparison of theoretical and experimental results. The theory and the applied numerical techniques have been described in a separate paper [1]. The basic circuitry of the balanced mixer that will be studied in depth in this paper is similar to that published by Dickens and Maki [6] and is sketched in Fig. 1. This mixer incorporates microstrip lines, slotlines, and coplanar waveguides, as well as some discontinuities. The theoretical and experimental analysis will take place in the LO frequency range of 1–15 GHz. In order to take the influence of the higher harmonic and mixing product impedances into account, an accurate description of the embedding network is required. In case of a balanced mixer, this network description is necessary for both of the mixer ports. For optimization of the embedding network (Section III), a description is required in which the network is split into its significant parts, such as different lines and discontinuities, and the performance of each part of the circuit is characterized by its physical parameters. Uniform lines will be described by their characteristic impedance and propagation constants, as given in published data. However, in case of discontinuities such as transitions and junctions between lines of different shape, the frequency-dependent characteristics are not available in general. Hence, some less important inhomogenities will be neglected. The error introduced by neglecting these discontinuities is small in the considered frequency range provided they are short compared with the wavelength. This is not true in the case of the nonuniform slotlines and microstrip lines to be used in some of our designs. In the appendix, it will be demonstrated that the nonuniform lines may be described through piecewise uniform lines yielding acceptable agreement between calculated and measured data. Assuming the transitions between microstrip line and coplanar waveguide, as well as the transition between slotline and coplanar waveguide, to be ideal, equivalent circuits for both of the mixer ports according to Fig. 2 can be supposed.

Manuscript received April 2, 1985; revised August 12, 1985.

The author is with the Technische Universität Berlin, Institut für Hochfrequenztechnik, Einsteinufer 25, D-1000 Berlin 10, West Germany.

IEEE Log Number 8405929.

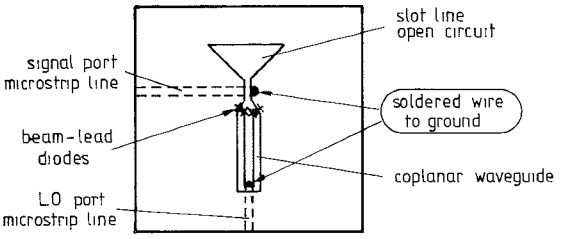

Fig. 1. Basic layout of the balanced mixer configuration.

The mixers were fabricated on a 1×1-in 0.635-mm-thick alumina substrate, the diodes were beam-lead Schottky diodes ALPHA DMF 5817A. The characteristic data of this diode are

$$I_s = 0.5 \cdot 10^{-7}\text{A};\ \eta = 1.08;\ \gamma = 0.5;\ \psi = 0.6\ \text{V};$$
$$C_{j0} = 0.25\ \text{pF};$$
$$C_p = 0.1\ \text{pF};\ L_S = 0.1\ \text{nH};\ R_S = 2.5\ \Omega$$

which are taken from measurements and data sheets. The transducer conversion loss will be used here which is given by

$$L = \frac{\text{power available from signal source}}{\text{power delivered to IF load}}.$$

The IF is chosen to be $f_{IF} = 30$ MHz, except in the case of mixing product recovery (Section V).

II. Conversion Loss of Fundamental and Harmonic Balanced Mixers

In this section, particular consideration will be given to the difference between fundamentally and harmonically pumped mixers. Even though it is not often necessary in the considered frequency range to make use of a harmonic mixer, it is interesting to demonstrate the usefulness of the numerical technique in describing such a configuration, especially for application to millimeter-wave problems.

If we first consider a balanced mixer as sketched in Fig. 1, the calculated and measured conversion losses for a fundamental mixer are as shown in Fig. 3. Reasonable agreement is obtained between theoretical and experimen-

0018-9480/86/0100-0120$01.00 ©1986 IEEE

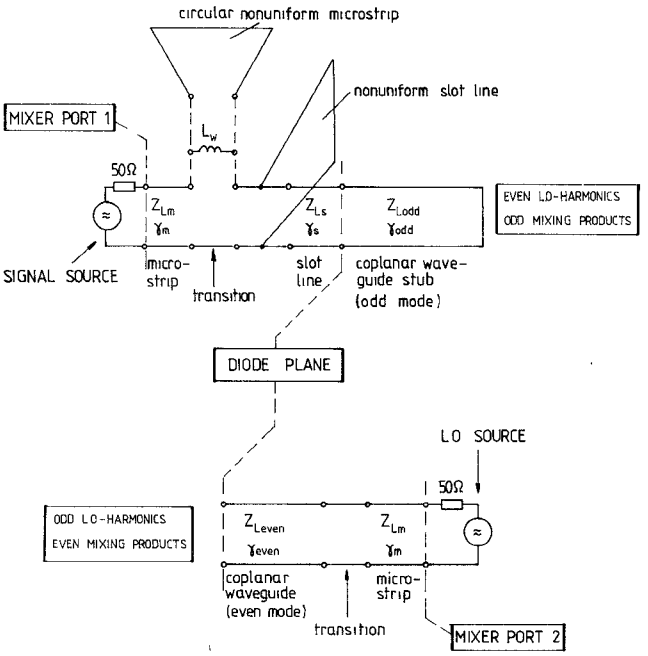

Fig. 2. Simplified equivalent circuits of the balanced mixer configuration.

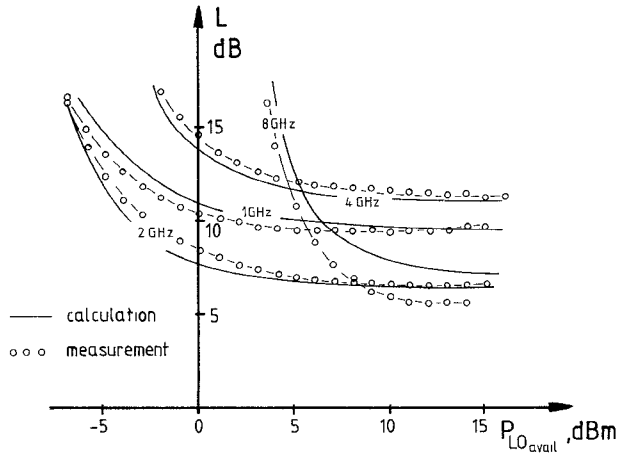

Fig. 3. Conversion loss against available LO power for the fundamental mixer of Fig. 1 with various signal frequencies.

tal results in a large LO power range for various frequencies.

Assuming the LO is applied at port 2 of the balanced mixer configuration, harmonic mixers are only realizable with an odd number of harmonics. If we consider a balanced mixer according to Fig. 1 pumped by the third harmonic, an LO power dependent conversion loss is obtained as given in Fig. 4, yielding good agreement between theory and experiment. The increased loss in the LO power range of 0 dBm is due to an efficient conversion to the dominant mixing products (sum and difference frequency) in conjunction with absorption in the according load impedances.

In conclusion, we can state that the conversion loss of a balanced mixer has been reasonably predicted as a function of LO power.

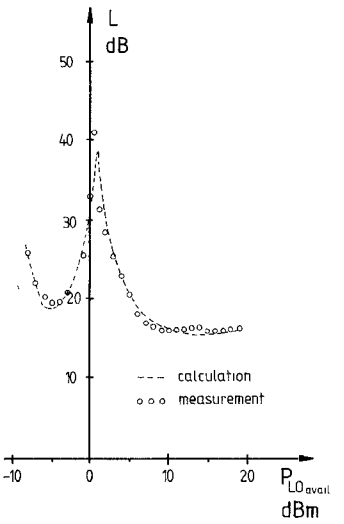

Fig. 4. Conversion loss against available LO power for the mixer of Fig. 1 pumped with the third subharmonic with signal frequency $f_S = 5$ GHz.

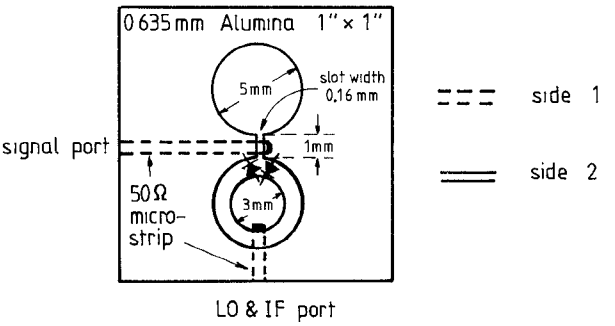

Fig. 5. Balanced mixer layout with soldered microstrip/slotline transition.

III. CAD of a Multioctave Balanced Mixer

The basic balanced mixer circuit considered here is equivalent to that given in Fig. 1. Without any optimization, this circuit yields a typical bandwidth of about two octaves. The aim of this chapter is to demonstrate the bandwidth improvement of this basic mixer circuit by means of a CAD technique.

It will be shown that the keys for bandwidth improvement are an optimization of the microstrip/slotline transition and the choice of optimal slotline parameters such as length and width.

In order to keep discontinuities as small as possible the basic mixer layout has been rearranged using circular line shapes as sketched in Fig. 5. The equivalent circuits of both mixer ports (Fig. 2) have been rearranged correspondingly. As mentioned above, the nonuniform lines will be treated as piecewise uniform lines. The validity of such a network description has been examined separately by comparing calculated results with measurements using an automatic network analyzer (see Appendix). It has been found that even the case of a nonuniform slotline can be described satisfactorily by this modeling technique.

Numerical calculations have been carried out in order to determine the optimal diameter of the slotline open circuit

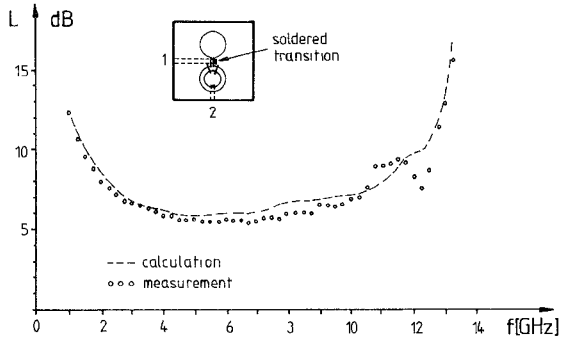

Fig. 6. Balanced mixer with soldered microstrip/slotline transition: Conversion loss against signal frequency, $P_{\text{LO avail}} = +10$ dBm.

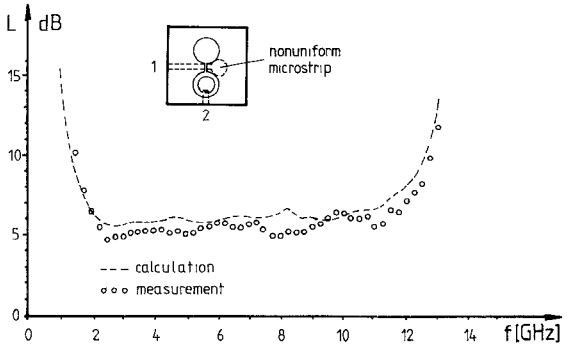

Fig. 8. Balanced mixer with nonuniform microstrip line: Conversion loss against signal frequency, $P_{\text{LO avail}} = +10$ dBm.

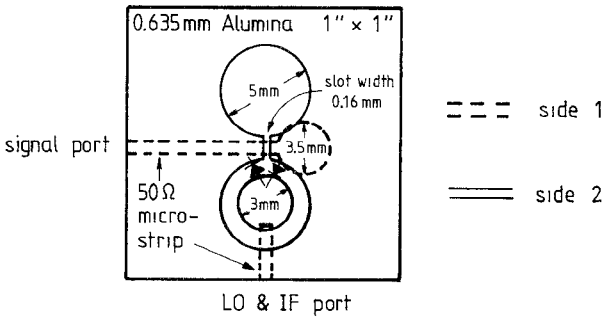

Fig 7. Balanced mixer layout with nonuniform microstrip line.

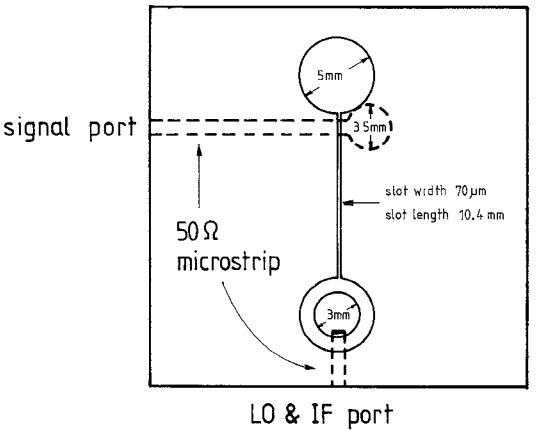

Fig. 9 Balanced mixer layout with extended slotline length.

for the desired frequency range of 2–12.5 GHz. As a result, the optimum diameter has been found to be approximately $d_s = 5$ mm, valid for alumina substrate of 0.635-mm thickness. A rigorous mixer calculation referring to [1] yields a frequency-dependent conversion loss for an available LO power of +10 dBm as given in Fig. 6; the corresponding measurements are also presented in this figure. For network analysis, the circular coplanar waveguide is treated as two independent slot lines.

Good agreement has been obtained between theory and experiment, except at the upper band limits. This is due to the fact that an exact description of a fundamental mixer requires an accurate embedding network description up to about the third or fourth harmonic, which is not possible using the simple equivalent circuits described above. However, the embedding network is well described in the lower frequency range, and the agreement between theory and experiment is within about 0.5 dB in this range.

A. Optimization of the Microstrip/Slotline Transition

A significant bandwidth improvement can be obtained if the soldered short at the end of the signal-port microstrip line is replaced by a virtual short through a circular nonuniform line (see Fig. 7). This virtual short, in conjunction with the virtual open of the circular slotline and the shorted stub through the coplanar waveguide, causes a reactance compensating effect [7]. Mixer calculations have been carried out to determine the optimum diameter d_m of the circular microstrip line. For the desired frequency range of 2–12.5 GHz, the optimum value has been found to be approximately $d_m = 3.5$ mm. It can be shown by calculation and experiment that a simple microstrip/slotline transition with a circular microstrip added will not exhibit the same broad-band characteristics as this mixer configuration.

Calculated and measured results are given in Fig. 8. It is noticeable, that the flatness of the frequency response is increased and the bandwidth is improved. Other combinations of circular slot stub and microstrip stub diameters have been calculated and measured yielding quite a similar agreement between theory and experiment but shall not be considered here.

B. Optimizing the Slotline Parameters

We shall now investigate the transformation effects due to the signal port slotline. In the case of a symmetrical extension of the slotline, calculations yield a decreased bandwidth, whereas in the unsymmetrical case (see Fig. 9), a further increase of bandwidth, depending on the slotline length and width, is predicted by numerical calculations. These calculations and the corresponding measurements of a fabricated mixer with a slotline length of 10.4 mm and a slot width of 70 μm are presented in Fig. 10.

The specifications of this final mixer configuration are

$$L = 6\,\text{dB} \pm 1\,\text{dB}$$

in the frequency range of 1.5–12.75 GHz yielding a bandwidth of 3.1 octaves.

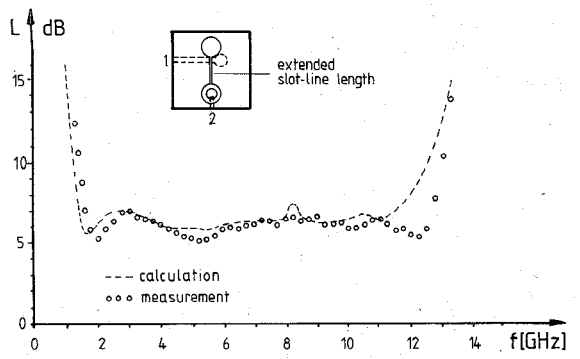

Fig. 10. Balanced mixer with extended slotline length: Conversion loss against signal frequency, $P_{\text{LO avail.}} = +10$ dBm.

IV. Influence of Diode Parameters on the Conversion Loss

In this section, the influence of the diode's series resistance R_S and the junction capacitance C_{j0} on the conversion loss of a balanced mixer will be studied theoretically and experimentally.

In order to provide a more general understanding, the calculations have been carried out using an ideal equivalent circuit of the balanced mixer. Let us assume a balanced mixer configuration without any band-limiting embedding circuitry. In this case, the nonlinear problem to be solved is simply given by the lumped-element description of the diode containing the diode's parasitics in conjunction with harmonic impedance conditions given by

$$Z_{\text{EMB}}(2\nu\omega_p) = \frac{1}{2}\cdot 50\ \Omega \quad Z_{\text{EMB}}\left[(2\nu-1)\omega_p\right] = 2\cdot 50\ \Omega.$$

Consequently, all mixing products are assumed to be terminated with a 50-Ω load.

A. Series Resistance R_S

In order to demonstrate the influence of the diode's series resistance R_S on the conversion loss of a mixer separately, it is useful to neglect all the other diode's parasitics. This can be arranged by applying rather low frequencies to the mixer diodes. For different values of R_S in the range of 0–20 Ω, the conversion loss can be calculated. These calculations have been carried out for different diodes (GaAs and Si) and a wide LO power range. The results can be summarized in Fig. 11, where the increase of the conversion loss is given, normalized to its value for $R_S = 0$. Note that this diagram is valid for Schottky diodes of different barrier height and a wide LO power range (medium barrier: $P_{\text{LO avail.}} > 0$ dBm; high barrier: $P_{\text{LO avail.}} > 6$ dBm). From Fig. 11, it is seen that an increase of conversion loss of 0.12 dB/Ω can be expected in the case of a balanced mixer and of 0.15 dB/Ω in the case of a single-ended mixer. In order to verify these predictions experimentally, a mixer configuration was considered which is similar to that given in Fig. 7. Two identical mixers have been fabricated but have been equipped with different diodes: a silicon *S*-band diode ($R_S \approx 2\Omega$; $C_{j0} \approx 0.35$ pF) and a silicon *Ku*-band diode) ($R_S \approx 21\ \Omega$; $C_{j0} \approx 0.05$ pF).

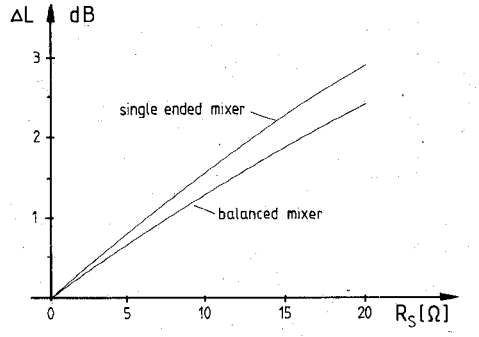

Fig. 11. Increase in conversion loss due to a series resistance R_S, calculated for the range of optimal LO power.

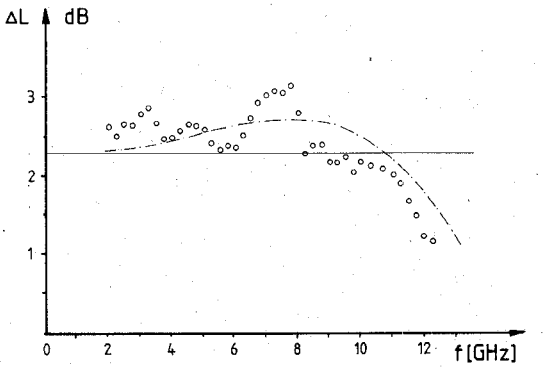

Fig. 12. Conversion loss difference of two equal mixers due to a different series resistance $\Delta R_S = 19\ \Omega$, calculated and experimental results. — —— frequency-independent solution referring to Fig. 11. ····· rigorous solution. OOO measurement.

According to the difference of $\Delta R_S = 19\ \Omega$ and referring to Fig. 11, we can expect a conversion loss difference between the mixers of typically $\Delta L \approx 2.3$ dB. For the frequency range of $f = 2$–12 GHz, the difference ΔL between the mixers is shown in Fig. 12. Comparing the experimental results with the theoretical values derived from the above-mentioned frequency-independent consideration, it can be seen that the order of magnitude of ΔL is reasonably predicted. Taking the different diode's reactances into account and considering the network characteristics yields theoretical results as given by the dashed curve.

As a result, it is noticeable that an *S*-band diode with a low series resistance and a rather high junction capacitance yields better mixer performance than a *Ku*-band diode having a high series resistance in conjunction with a rather low junction capacitance even up to upper *X*-band frequencies. This effect will be studied in depth in Section IV-C.

B. Junction Capacitance C_{j0}

As we have considered a variation of the series resistance R_S assuming that no change of the barrier capacitance C_{j0} takes place simultaneously, let us now consider a variation of C_{j0} assuming R_S to be constant. It is obvious that, in practice, a change of C_{j0} due to the junction diameter causes a change of R_S. However, let us neglect this effect at this time and treat it separately in Section IV-C. Calculations have been carried out for a balanced mixer with an

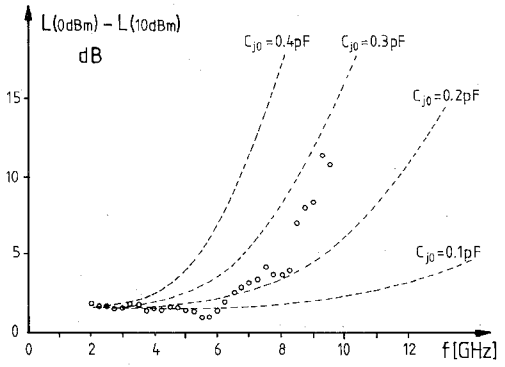

Fig. 13. Conversion loss difference for an LO power change from 0 to 10 dBm calculated for Si Schottky-barrier diode DMF 5817A. --- calculations. ○○○ measurements.

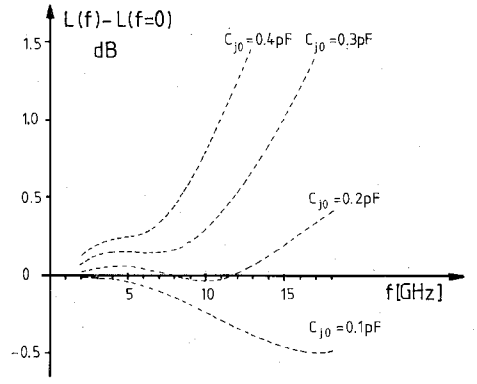

Fig. 14. Frequency-dependent conversion loss difference, normalized to low-frequency values, calculated for Si Schottky-barrier diode DMF 5817A and an LO power of +10 dBm.

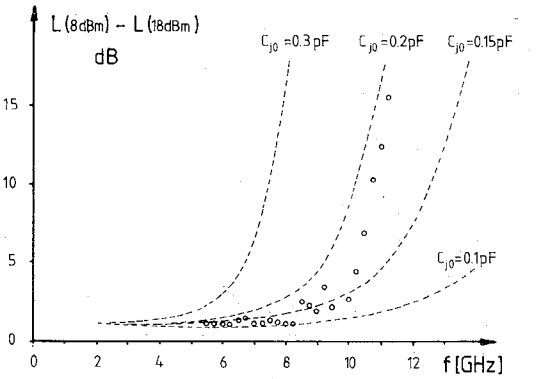

Fig. 15. Conversion loss difference for an LO power change from 8 to 18 dBm calculated for GaAs Schottky-barrier diode DMK 6604A. --- calculations. ○○○ measurements.

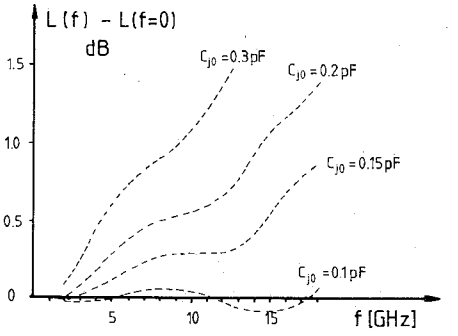

Fig. 16. Frequency-dependent conversion loss difference, normalized to low-frequency values, calculated for GaAs Schottky-barrier diode DMK 6604A and an LO power of +18 dBm.

ideal embedding network as defined above, where two different diagrams shall be considered. The first diagram shows the frequency-dependent increase of the conversion loss, when the LO power is reduced from an optimum value to a level which is 10 dB below this optimum. As large differences of the conversion loss occur in this case, this presentation is well suited for a comparison between calculated and measured results. A second diagram shows the frequency-dependent conversion loss compared with the conversion loss at low frequencies, calculated for an optimum LO power.

For an *S*-band silicon Schottky-barrier diode ALPHA DMF 5817A, the results are plotted in Figs. 13 and 14. Experimental results are included in Fig. 13 yielding a value of $C_{j0} \approx 0.25$ pF being in good agreement with measured values of $C_{j0} = 0.25$–0.3 pF determined from $1/C^2 = f(U_D)$ measurements which have been carried out with an automatic network analyzer. Regarding Fig. 14, it should be noted that a decrease of the conversion loss in case of $C_{j0} < 0.2$ pF is due to matching conditions at the signal and/or IF port.

For an *X*-band GaAs Schottky barrier diode ALPHA DMK 6604A the results are plotted in Figs. 15 and 16. The experimental data are included in Fig. 15 yielding a value of $C_{j0} \approx 0.15$–0.2 pF.

The parameters of this GaAs diode are

$$I_S = 1.2 \cdot 10^{-14}\text{A};\ \eta = 1.17;\ \gamma = 0.5;\ \psi = 0.85\text{V};$$
$$C_{j0} = 0.15\text{pF};$$
$$C_p = 0.1\text{pF};\ L_S = 0.1\text{nH};\ R_S = 1.5\ \Omega$$

which are taken from measurements and data sheets.

Comparing Figs. 14 and 16, it is noticeable that the frequency dependence of the conversion loss in the frequency range up to 15 GHz at optimal LO power (+10 dBm for the *S*-band Si diode and +18 dBm for the *X*-band GaAs diode) does not differ significantly between the two diodes, which is in good agreement with experimental results.

C. *Influence of the Time Constant* $\tau = R_S C_{j0}$

In real Schottky-barrier diodes the junction capacitance C_{j0} and the series resistance R_S are connected physically through the junction area A. Following [8], the series resistance is given by

$$R_S = \underset{\sim \frac{1}{\sqrt{A}}}{R_{\text{substrate}}} + \underset{\sim \frac{1}{A}}{R_{\text{epilayer}}} + R_{\text{contacts}}.$$

Depending on the diode's construction two cases shall be

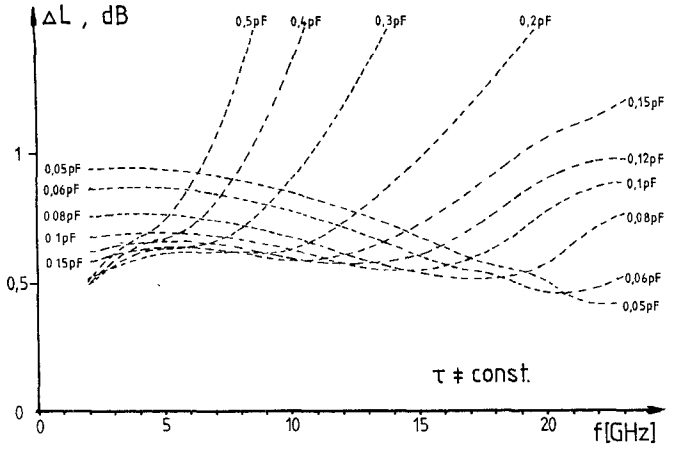

Fig. 17. Frequency-dependent increase of the conversion loss when varying the junction area, assuming a dominant substrate resistance.

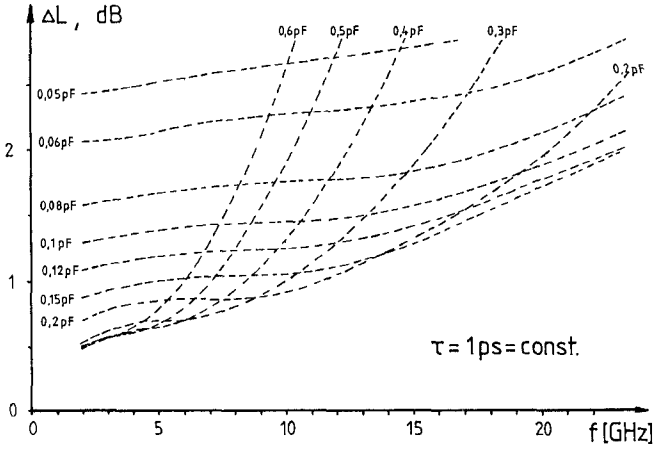

Fig. 18. Frequency-dependent increase of the conversion loss when varying the junction area, assuming a dominant epilayer resistance.

TABLE I

frequency band	[GHz]	C_{j0}[pF]	R_S[Ω]	τ[ps]
D	1–2	0.4	2.5	1
S	2–4	0.25	3.2	0.8
C	4–8	0.2	3.5	0.7
X	8–12	0.15	4.1	0.62
Ku	12–18	0.1	5	0.5
K	18–26	0.06	6.5	0.39

considered:

1) R_S dominated through substrate resistance;
2) R_s dominated through epilayer resistance.

In conjunction with the capacitance C_{j0} being proportional to the junction area A, we have a time constant in the two cases given by

1) $\tau = R_S C_{j0} \sim \sqrt{A}$
2) $\tau = R_S C_{j0} = \text{const.}$

Assuming a diode for low frequencies having a $C_{j0} = 0.4$ pF and an $R_S = 2.5\ \Omega$ ($\tau = 1$ ps), we can study a decrease of the junction area through mixer calculations. Calculations have been carried out for the above-defined idealized balanced mixer with typical Si Schottky-barrier diode data and an LO power of +10 dBm. The results are normalized to those for ideal diodes ($R_S = C_{j0} = 0$). In the case of a dominant series resistance due to the substrate resistance (case 1, $\tau \neq$ const), we get an assumed range of

$$R_S = 2.5\text{–}7.07\ \Omega$$
$$C_{j0} = 0.4\text{–}0.05\ \text{pF}$$

yielding a frequency dependence of the conversion loss as given in Fig. 17. From this figure, optimal diodes for different frequency bands can be obtained which are given in Table I.

In the case of a dominant series resistance due to the epilayer resistance (case 2, $\tau = \text{const}$), which seems to be a more realistic assumption [8], we get an assumed range of

$$R_S = 2.5\text{–}20\Omega$$
$$C_{j0} = 0.4\text{–}0.05\text{pF}$$

yielding a frequency-dependent increase of the conversion loss as given in Fig. 18. Optimal combinations for different frequency bands can be obtained from this figure which are given in Table II.

TABLE II

frequency band	[GHz]	C_{j0}[pf]	R_S[Ω]	τ[ps]
S	2–4	0.4	2.5	1
C	4–8	0.3	3.3	1
X	8–12	0.2	5	1
Ku	12–18	0.15	6.6	1
K	18–26	0.12	8.3	1

Comparing the values between Tables I and II, it is seen that the optimal series resistances for the different frequency bands do not differ as much as the optimal junction capacitance values. Hence, we can state that the influence of the series resistance on the conversion loss seems to be more important than the influence of the junction capacitance. This statement is in good agreement with several experimental results where a low-cost *S*-band Si Schottky-barrier diode yielded conversion losses up to 14 GHz which did not differ significantly from those achieved with *X*-band GaAs–Schottky-barrier diodes.

Quite similar results have been obtained when calculating single-ended mixers but this will not be discussed in detail here.

V. Mixing Product Recovery

In the field of microwave and millimeter-wave mixers, mixing product recovery techniques have been used in order to reduce the conversion loss by means of re-mixing. However, some of these image- and/or sum-enhanced mixers yield conversion-loss improvements which have only been qualitatively explained by idealized theoretical considerations.

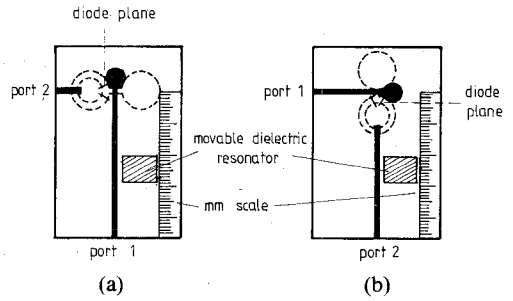

Fig. 19. Planar balanced mixer layout (a) for image recovery and (b) for sum and sum–image recovery.

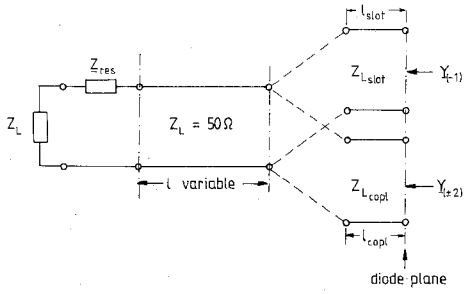

Fig. 20. Simplified equivalent circuit for the sideband under consideration when using the mixing product recovery technique.

This section is intended to show how much conversion loss improvement can be achieved by various recovery techniques at microwave frequencies. The mixing product recovery will be studied for image–sum $(2f_p + f_{IF})$ and sum–image $(2f_p - f_{IF})$ by means of movable dielectric resonators (see Fig. 19) which are tuned to the sideband under consideration. Due to the mixing product splitting of a balanced mixer, two different mixers have been fabricated (Fig. 19(a) and (b)). The only difference between these configuration is the extended length of the microstrip line at port 1 or port 2.

In the case of a dielectric resonator, the electrical properties at resonance may be described by a purely resistive impedance. Network analyzer measurements have been carried out and the resonance impedances of the incorporated dielectric resonators have been found to be within $500\ \Omega \leqslant Z_{res} \leqslant 1000\Omega$ if the distance between the resonator and the microstrip line remains constant. The equivalent circuit valid for the mixing product under consideration may be described by Fig. 20, where the movement of the resonator is described by a variable line length inserted between the resonator and the diode plane.

Calculations and measurements have been carried out in the frequency range of 3.5–4.5 GHz. The IF is chosen to be 100 MHz in order to achieve large frequency differences between the mixing products. The diodes are ALPHA DMF 5817A and the LO power is chosen to be +10 dBm. Theoretical and experimental data will be normalized to the conversion loss without resonator which is typically $L \approx 5.5$ dB.

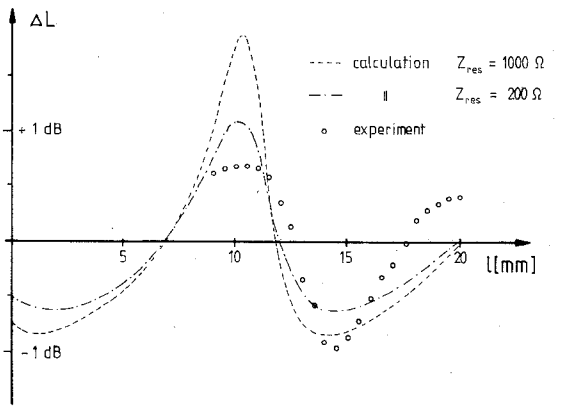

Fig. 21. Theoretical and experimental results for image recovery.

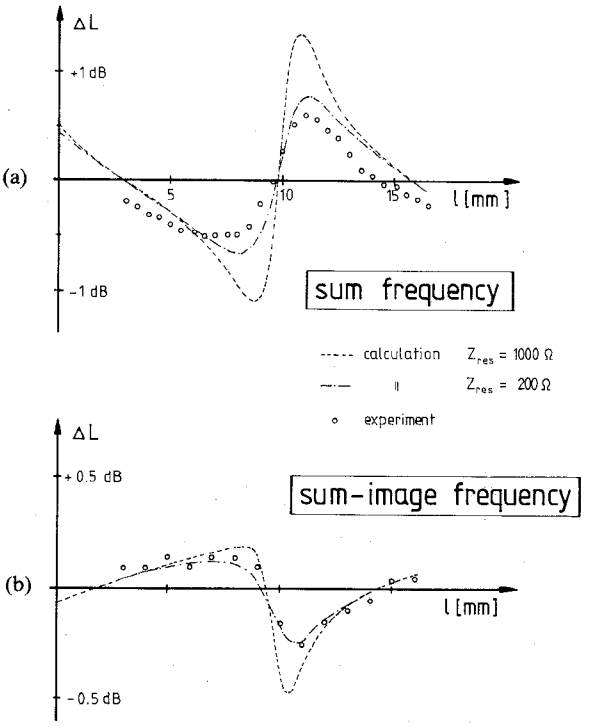

Fig. 22. Theoretical and experimental results for (a) sum and (b) sum–image recovery.

A. Image Recovery

In the case of an image recovery mixer, the configuration of Fig. 19(a) has to be used. Experimental results are shown in Fig. 21. The theoretical results that are also given in this figure are calculated for two different resonance impedances. It can be seen that reasonable agreement between theory and experiment has been obtained if the resonance impedance is assumed to be $Z_{res} = 200\ \Omega$. The conversion-loss improvement as predicted by numerical calculations is about 1 dB. It should be pointed out that the improvement of the conversion loss is of the same order of magnitude as predicted by some simplified theoretical treatments of this problem [9], [10]. However, experimental results have been published where conversion-loss improvements are reported which are significantly higher [11], [12].

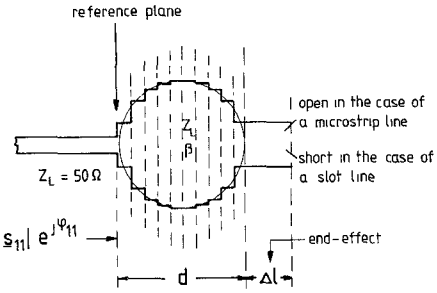

Fig. 23. Basic configuration and equivalent circuit overlay of a circular stub.

B. Sum and Sum–Image Recovery

In case of the sum and sum–image recovery, the configuration of Fig. 19(b) has to be used because both of these sidebands occur at the mixer port 2. Theoretical and experimental results for sum recovery are given in Fig. 22(a); good agreement can be observed. A conversion-loss improvement of 0.5 dB has been obtained for this recovery technique.

The results for sum–image recovery are given in Fig. 22(b), yielding a conversion-loss improvement of about 0.25 dB.

Note that an improvement of the conversion loss by means of sum recovery ($l \approx 8$ mm) would cause a deterioration by means of sum–image recovery if a resonator of low Q is applied. Consequently, it should be mentioned that sum recovery yields an optimal improved conversion loss only if a simultaneous sum–image recovery with the same phase of the reflection coefficient is avoided.

VI. Conclusion

It has been demonstrated in this paper that various mixer problems can be described and optimized through a CAD technique incorporating a numerical technique based on theoretical considerations as given in [1]. Due to the good convergence of the proposed nonlinear mixer analysis, systematical variations of different circuit parameters can be studied.

A run of the nonlinear analysis on a CYBER 170-835 requires typically about 0.23 s for one LO cycle, if a voltage-dependent junction capacitance is included in the analysis, which yields a total calculation time of 2–4 s for each value of the conversion loss.

Appendix
Line Theory Modeling of Nonuniform Lines

The application of tuning stubs with characteristic impedances differing from that of the input and output lines (i.e., 50 Ω) leads to parasitic reactances at the connection planes. Thus, it is advantageous to use nonuniform lines in order to realize slight changes of the line shape instead of step discontinuities.

Distinguishing both of the tuning stubs as applied in Section III, circular line shapes are to be preferred instead of rectangular line shapes (see Figs. 5 and 7). These circular line shapes can be described as piecewise uniform lines. However, the basic question is whether reasonable agreement between calculated and measured data can be achieved. This Appendix is intended to describe the circuit models used and give a comparison between calculated results and measured data.

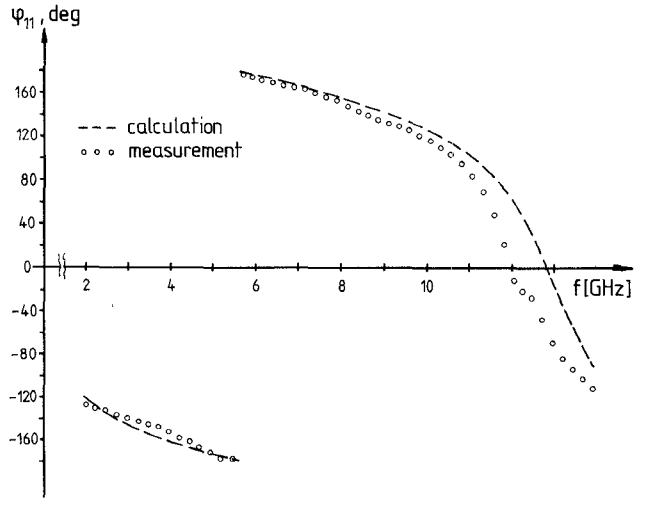

Fig. 24. Phase response φ_{11} against frequency for a circular microstrip line of 4.5-mm diameter.

Let us consider a basic configuration as sketched in Fig. 23. Its electric behavior may be described by the equivalent circuit which is included in this figure. The circular stub, which is represented by a stepped line with 20 line segments of equal length, is terminated by a line of length Δl, describing the open end effect of the microstrip and the end effect of the shorted slotline, respectively.

It is obvious that a reactance line may be characterized by regarding the phase response of the input reflection coefficient $\varphi_{11}(f)$. Using a network analyzing computer program, this phase response is calculated at the reference plane, varying frequency from 2 GHz to 14 GHz.

A. Circular Microstrip Stub

The characteristic impedance, effective dielectric constant, dispersion characteristics, and the equivalent line Δl of the open end effect are calculated with separate computer programs [13], [14]. For a diameter of $d = 4.5$ mm, the results are plotted in Fig. 24 as an example.

The measurements have been carried out using an automatic network analyzer system. Using the well-known calibration techniques, the reference plane has been chosen to be at the edge of the circular microstrip line. It can be seen from Fig. 24 that good agreement has been obtained between calculated and measured data. Calculations and measurements have been carried out for a set of eight different circular microstrip lines (3.0–6.5-mm diameter) yielding quite a similar agreement between calculated and measured results as given in Fig. 24.

When comparing theoretical and experimental data, the relevance of the equivalent circuit of Fig. 23 has been demonstrated for a circular microstrip stub.

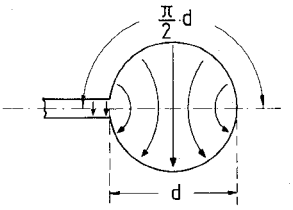

Fig. 25. Electrical field distortion for a circular slot stub.

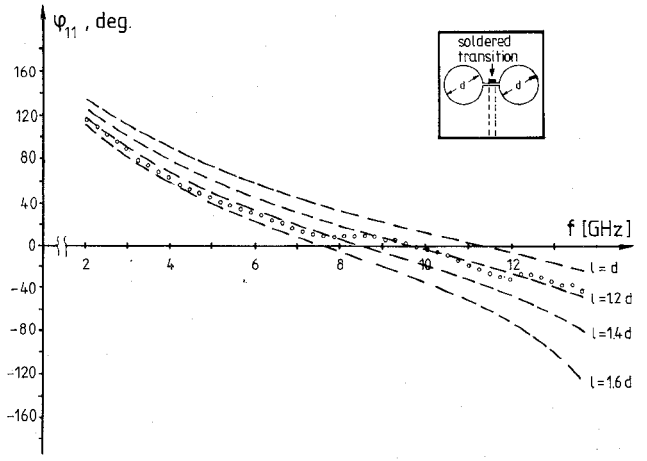

Fig. 26. Phase response φ_{11} against frequency for *two* circular slot stubs connected in parallel (diameter $d_S = 4$ mm). --- calculated results using the equivalent circuit of Fig. 23 with various values of length l ○○○ measured data.

B. Circular Slot Stub

In the case of an inhomogeneous slotline, its treatment using the equivalent circuit shown in Fig. 23 is more difficult. The main reason for this is a significant field distortion as sketched in Fig. 25 for the transverse electrical field.

Moreover, due to this field distortion, the question arises which effective physical length has to be assumed: either the diameter d or half the circumference $u = (\pi/2)d$. The answer will be given by comparing theoretical and experimental results.

The characteristic impedances and dispersion characteristics are calculated in a separate computer program based on a mode-matching technique [15].

The network calculations were carried out for two circular slot stubs connected in parallel (as included in Fig. 26) in order to simplify the measurements. The frequency dependence of the characteristic impedance of the slotline has been neglected. The phase response φ_{11} is calculated by varying the physical line length between $l = d$ and $l = 1.6\ d$; the results are plotted in Fig. 26.

The measurements have been carried out for the configuration of Fig. 26, where the reference plane is at the ground metallization.

It can be seen from Fig. 26 that good agreement between theoretical and experimental data can be obtained by choosing the physical line length to be $l \approx 1.5\ d$. Thus, we can state that the effective physical length is about half the circumference, and for all calculations here we assume $l = 1.5\ d$. Comparing the theoretical and experimental results of a set of five different circular slotlines (4.0–6.0-mm diameter) yields quite similar conditions. Due to the fact that we use this equivalent physical length, it is not necessary to include an additional line length Δl describing the end effect of the shorted slotline.

Thus, the validity of the equivalent circuit of Fig. 23 has been demonstrated even for the case of two circular slotlines connected in parallel.

Acknowledgment

Thanks are due to Prof. John for having initiated this work and for encouragement during the course of this research project. Also, the author gratefully acknowledges the financial support of the Deutsche Forschungsgemeinschaft which has enabled the author to study in depth some aspects of the broad-band circuitry of Section III.

References

[1] B. Schüppert, "A fast and reliable method for computer analysis of microwave mixers," this issue, pp. 110–119.
[2] D. N. Held and A. R. Kerr, "Conversion loss and noise of microwave and millimeter-wave mixers. Parts 1+2," *IEEE Trans. Microwave Theory Tech.*, vol. MTT-26, pp. 49–61, 1978.
[3] D. H. Held, "Analysis of room temperature millimeter-wave mixers using GaAs Schottky barrier diodes," Sc.D. dissertation, Dept. Elec. Eng. Columbia Univ., New York, 1976.
[4] P. H. Siegel and A. R. Kerr, "The measured and computed performance of a 140–220 GHz Schottky diode mixer," *IEEE Trans. Microwave Theory Tech.*, vol. MTT-32, pp. 1579–1590, 1984.
[5] S. J. Nightingale, "Loss and noise characteristics of microwave mixers," Philips Res. Rep. No. 3162, Redhill, 1980.
[6] L. E. Dickens and D. W. Maki, "An integrated-circuit balanced mixer, image and sum enhanced," *IEEE Trans. Microwave Theory Tech.*, vol. MTT-23, pp. 276–281, 1975.
[7] G. Oltman, "The compensated balun," *IEEE Trans. Microwave Theory Tech.*, vol. MTT-14, pp. 112–119, 1966.
[8] N. P. Cerniglia et al., "Beam-lead Schottky-barrier diodes for low-noise integrated microwave mixers," *IEEE Trans. Electron Devices*, vol. ED-15, pp. 674–678, 1968.
[9] H. C. Torrey and C. A. Whitmer, *Crystal Rectifiers* (MIT Radiation Lab. Series, vol. 15). New York: McGraw-Hill, 1948.
[10] A. A. M. Saleh, *Theory of Resistive Mixers*. Cambridge MA: MIT Press, 1971.
[11] T. H. Oxley *et al.* "Image recovery mixers," in *2nd Eur. Microwave Conf.*, 1971, pp. A11/5:1–A11/5:4.
[12] J. P. Fekete, "Image recovery microwave mixer," in *2nd Eur. Microwave Conf.*, 1971, pp. A12/1:1–A12/1:4.
[13] E. Hammerstad and O. Jensen, "Accurate models for microstrip computer-aided design," in *1980 IEEE MTT-S Int. Microwave Symp. Dig.*, (Washington), 1980, pp. 407–409.
[14] M. Kirschning *et al.*, "Accurate model for open end effect of microstrip lines," *Electron. Lett.*, vol. 17, pp. 123–125, 1981.
[15] J. Siegl, "Numerische Berechnung der Grundwelle und der höheren Wellentypen auf einer Schlitzleitung mit rechteckigem Schirm und endlicher Metallisierungsdicke," Dissertation, Institut für Hochfrequenztechnik, Technische Universität Berlin, 1978.

✠

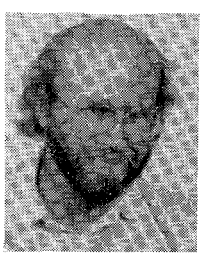

Bernd Schüppert was born June 5, 1947, in Neunkirchen, West Germany. He received the Dipl.-Ing. degree (1978) and the Dr.-Ing. degree (1983), both in electrical engineering, from the Technische Universität Berlin.

Since 1978, he has been a Research Associate at the Technische Universität Berlin, Institut für Hochfrequenztechnik, working on mixer problems, both theoretically and experimentally. During 1983–1984, he worked on a research project on planar balanced broad-band mixers, sponsored by the Deutsche Forschungsgemeinschaft. Since 1983, he has been working on Ti:$LiNbO_3$ integrated optic devices as a head of the technology group at the Institut für Hochfrequenztechnik.

Dr. Schüppert is a member of the VDE/NTG (Germany)